Accepted Manuscript

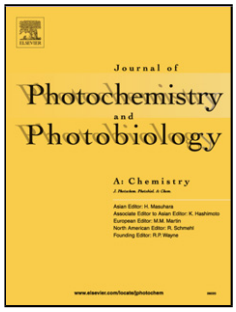

Title: A new "ON-OFF" fluorescent and colorimetric chemosensor based on 1,3,4-oxadiazole derivative for the detection of Cu^{2+} ions

Authors: Lin Wang, Qijing Bing, Jianxin li, Guang Wang

PII: S1010-6030(18)30261-2
DOI: https://doi.org/10.1016/j.jphotochem.2018.04.015
Reference: JPC 11230

To appear in: *Journal of Photochemistry and Photobiology A: Chemistry*

Received date: 25-2-2018
Revised date: 23-3-2018
Accepted date: 7-4-2018

Please cite this article as: Lin Wang, Qijing Bing, Jianxin li, Guang Wang, A new "ON-OFF" fluorescent and colorimetric chemosensor based on 1,3,4-oxadiazole derivative for the detection of Cu2+ ions, Journal of Photochemistry and Photobiology A: Chemistry https://doi.org/10.1016/j.jphotochem.2018.04.015

A new "ON-OFF" fluorescent and colorimetric chemosensor based on 1,3,4-oxadiazole derivative for the detection of Cu^{2+} ions

Lin Wang, Qijing Bing, Jianxin li, Guang Wang*

Faculty of Chemistry, Northeast Normal University, Changchun 130024, P. R. China

Corresponding author: Guang Wang

Tel: 86+431+85099544;

Fax: 86+431+85098768.

E-mail : wangg923@nenu.edu.cn (G. Wang)

Graphical Abstract

Highlights

- A new "ON-OFF" fluorescent and colorimetric chemosensor based on 1,3,4-oxadiazole derivative for the detection of Cu^{2+} ions
- Lin Wang, Qijing Bing, Jianxin Li, Guang Wang*
- *Faculty of Chemistry, Northeast Normal University, Changchun 130024, P. R. China*
- ► Pyrazole-containing oxadiazole derivative as fluorescent chemosensor (sensor 1) was synthesized successfully.
- ► Sensor 1 displayed high selective and sensitive fluorescence sensing for Cu^{2+}.
- ► Sensor 1 showed high anti-interference ability in the co-existence of other metal ions.
- ► Sensor 1 also showed the ability of naked-eye detection for Cu^{2+} ions.

Abstract: A symmetrical oxadiazole derivative (OXD) containing two pyrazole moieties was synthesized successfully and characterized by single crystal X-ray diffraction, nuclear magnetic resonance and mass spectrometry. The synthesized

compound displayed “On-Off” fluorescent sensing towards Cu^{2+} with high selectivity and sensitivity. Fluorescence and UV-vis absorbance spectra studies demonstrated that the proposed sensor can detect Cu^{2+} directly in acetonitrile solution over a wide range of metal ions including Ag^{+}, Na^{+}, K^{+}, Hg^{2+}, Mg^{2+}, Cd^{2+}, Co^{2+}, Ni^{2+}, Zn^{2+}, Fe^{2+}, Pb^{2+}, Ca^{2+}, Mn^{2+}, Ba^{2+}, Fe^{3+}, Al^{3+}, and Cr^{3+}. Moreover, the synthesized sensor exhibits an instantaneous naked-eye color change from colorless to yellow with the presence of Cu^{2+} ion. The fluorescence intensity of the sensor has shown a linear response to Cu^{2+} in the concentration range of 0～15 μM with a detection limit of 2.14 μM. Fluorescence titration, ^{1}H NMR spectrum, ESI-MS, and DFT calculation confirmed that fluorescence quenching is caused by the complex formation between the sensor and Cu^{2+} with 1:1 stoichiometry.

Keywords: Chemosensor; Fluorescence; Colorimetric; Oxadiazole; Copper ion.

1. Introduction

As the third most abundant transition metal ion in the human body, copper ions plays pivotal roles as trace element in biological systems and process [1-2]. Cu^{2+} ion is one kind of the essential trace metal ion to sustain normal human health and serves as a cofactor for a wide variety of enzymes in all living organisms. Although Cu^{2+} ions are the essential trace elements after iron and zinc in the human body, they are harmful to humans and organisms at high concentration [3]. Copper ions can accumulate in the environment, which finally results in contaminated food and water. According to the World Health Organisation (WHO), 1 $mg \cdot L^{-1}$ is the maximum

acceptable limit of copper for drinking water. High Cu^{2+} concentration in neuronal cytoplasm can lead to Wilson's disease, Menkes's disease and Alzheimer's disease [4-5], overloading copper exhibits toxicity and causes irritation of nose and throat resulting in nausea, vomiting, and diarrhea [6]. The traditional detection methods for metal ions such as coupled plasma atomic emission spectrometry (ICP-AES) [7-8], atomic absorption spectroscopy (AAS) [9], fluorescence techniques [10] and electrochemical methods (EM) [11] require sophisticated equipment, tedious sample preparation procedures. In addition, these analytical instruments are expensive and need trained operators [12].

Compared to these traditional analytical methods, fluorescent chemosensors have many advantages such as real-time monitoring with fast response times, intrinsic high selectivity and sensitivity, ease of handling and low-cost [13-14]. Up to now, a lot of fluorescent and colorimetric chemosensors of Cu^{2+} based on small organic molecules, conjugated polymers, nanoparticles and biomolecules were reported [15-21]. Although the researchers have been made a lot of contribution to chemosensors, development of new fluorescent chemosensors with high sensitivity and selectivity for the detection of heavy metal ions in real samples is still urgent.

Most of oxadiazole derivatives have been used as fluorescent emitters for OLEDs due to their excellent photophysical properties and chemical stabilities [22-23]. Till now, to the best of our knowledge, only several reports are relative with the oxadiazole derivatives as fluorophore in chemosensor and presented excellent sensing

properties for metal ions [24-25]. So, further exploring new fluorescence chemosensors with high selectivity and sensitivity based on oxadiazole is significant.

On the basis of the above concept, we report herein a novel highly sensitive and selective "on-off" fluorescent chemosensor towards Cu^{2+} based on a 1,3,4-oxadiazole as the fluorophore and the pyrazole as the receptor (sensor **1** in Scheme 1). Sensor **1** contained two pyrazole units and presented symmetrical structure, which was hoped to provide special steric configuration and selectively coordinate with metal ion. The experimental results demonstrated that sensor **1** exhibited obvious fluorescence change and a clearly visible color change from yellow to colorless upon the addition of Cu^{2+} ions in acetonitrile medium.

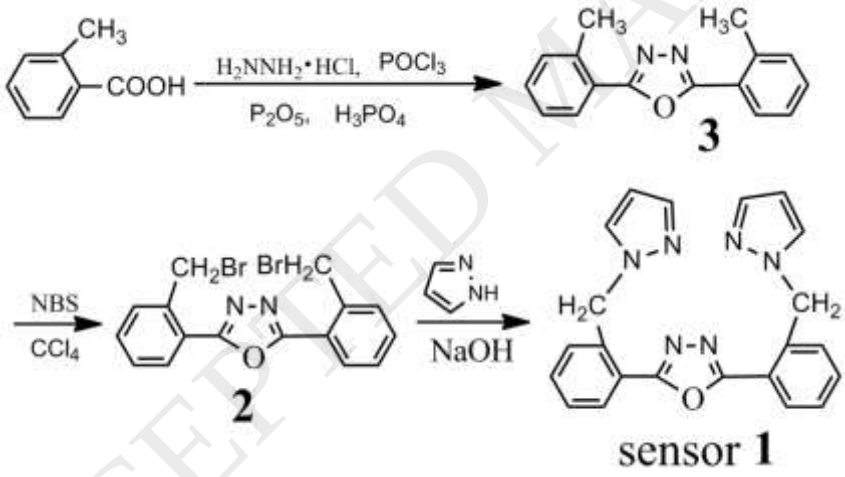

Scheme 1. The synthetic route of sensor **1**

2. Experimental

2.1. Materials and methods

All solvents were purchased from commercial sources and purified by standard methods. Pyrazole was bought from Aladdin Industrial Corporation and used without

further purification. All other chemicals were obtained from Sinopharm Chemical Reagent Co. Lid and were analytical grade reagent. Double-distilled water was used for all experiments. The salts used in stock solutions of metal ions are $CuCl_2 \cdot 2H_2O$, NaCl, $Ni(NO_3)_2 \cdot 6H_2O$, $Al(NO_3)_3 \cdot 9H_2O$, $MnCl_2.4H_2O$, $Zn(NO_3)_2 \cdot 6H_2O$, $Cr(NO_3)_3 \cdot 9H_2O$, $Cd(NO_3)_2 \cdot 4H_2O$, $Fe(NO_3)_3 \cdot 9H_2O$, $Co(NO_3)_2 \cdot 6H_2O$, $Mg(NO_3)_2 \cdot 6H_2O$, KNO_3, $AgNO_3$, $BaCl_2 \cdot 2H_2O$, $HgCl_2$, $PbCl_2$, $CaCl_2$ and $FeSO_4 \cdot 7H_2O$.

^1H NMR and ^{13}C NMR spectra were obtained on Varian Unity Inova Spectrometer 400 MHz. ESI-MS mass spectra were obtained on an agilent 1200 HPLC/Micro TOF Ⅱ mass spectrometer. UV-vis absorption and fluorescent spectra were recorded on Varian Cary 500 Spectrophotometer and Varian Cary Eclipse Fluorescence Spectrophotometer, respectively.

2.2. Synthesis and characterization

2,5-(2-methylphenyl)-1,3,4-oxadiazole (Compound **3)**

A mixture of *o*-toluic acid (6.8 g, 0.05 mol), hydrazine hydrochloride (2.6 g, 0.025 mol) and phosphoric acid (13.5 mL, 0.25 mol) in a 250 mL flask was stirred at room temperature. Phosphorus oxychloride (4.6 mL, 0.05 mol) and phosphorus pentoxide (21.3 g, 0.15 mol) were added dropwise into the above reaction mixture successively. The mixture was heated to 140 ℃ under stirring and nitrogen atmosphere for 2 h. After cooling to room temperature, the mixture was poured into ice water. The precipitate was obtained by filtration and washed with the solution of

$NaHCO_3$ (85%) and deionized water. The crude product was recrystallized from ethanol to give 2,5-(2-methylphenyl)-1,3,4-oxadiazole as a white crystal, 3.64 g, yield, 58.2%. ^{1}H NMR (600 MHz, $CDCl_3$) δ 8.04 (d, *J* = 7.5 Hz, 2H), 7.48 – 7.33 (m, 6H), 2.77 (d, *J* = 19.8 Hz, 6H). ^{13}C NMR ($CDCl_3$, 600MHz, ppm): 164.43, 138.51, 131.84, 131.21, 129.00, 126.23, 123.07, 22.23. HR-ESI MS calcd for $C_{16}H_{14}N_2O$ 250.30 (**3**$^+$, 100%), found 251.1185 *m/z* ([**3**+ H^+]$^+$).

2,5-bis [(2-bromomethyl)phenyl]-1,3,4-oxadiazole (Compound **2**)

2,5-(2-methylphenyl)-1,3,4-oxadiazole (2.0 g, 8 mmol) was dissolved in purified carbon tetrachloride (50 mL). After the solution was refluxed for 0.5 h under stirring, N-bromosuccinimide (NBS, 4.27 g, 24.0 mmol) and diphenylperoxyanhydride (BPO, 0.24 g, 0.01 mol) were added. The mixture was further refluxed for another 5 h. After the resulted mixture cooled down, the solvent was removed [25]. The residue was washed with hot water three times, dried under vacuum and recrystallized with THF and ethanol (THF:ethanol=1:1) to afford white solid of 2,5-bis [(2-bromomethyl)phenyl]-1,3,4-oxadiazole, 2.17 g, yield, 66.4%. ^{1}H NMR (400 MHz, $CDCl_3$, ppm) δ 8.14 (d, *J* = 7.6 Hz, 2H), 7.63 (d, *J* = 7.1 Hz, 2H), 7.53 (m, 4H), 5.20 (s, 4H). ^{13}C NMR ($CDCl_3$, 600MHz, ppm): 137.73, 132.15, 131.98, 129.65, 129.07, 100.00, 31.73. HR-ESI MS calcd for $C_{16}H_{12}Br_2N_2O$ 408.09 (**2**$^+$, 100%), found 408.9369 m/z ([**2**+ H^+]$^+$).

2,5-Bis[(2-pyrazolyl) methyl]-1,3,4-oxadiazole (sensor **1**).

A mixture of pyrazole (1.09 g, 16.0 mmol) and NaOH (0.64 g, 16.0 mmol) in deionized water (5 mL) was stirred under heating in an oil bath at 40 ºC for 5 min. 2,5-bis [(2-bromomethyl)phenyl]-1,3,4-oxadiazole (0.82 g, 2.0 mmol) in THF (10 mL) was added dropwise to the previous mixture in 10 min. The resulting solution was then heated to 70 ℃ for 24 h. The resulting mixture was cooled to room temperature, poured into water, and filtered. The crude product was further purified by column chromatography on silica gel (ethyl acetate: petroleum ether = 5:2) to give white solid, 0.43 g, yield, 56.8%. ^{1}H NMR (400 MHz, $CDCl_3$, ppm) δ 8.08 (m, 2H), 7.60 (d, *J* = 2.5 Hz, 4H), 7.49 (t, *J* = 5.4 Hz, 4H), 7.01 (d, *J* = 6.7 Hz, 2H), 6.32 (t, *J* = 2.1 Hz, 2H), 5.99 (s, 4H); ^{13}C NMR ($CDCl_3$, 600MHz, ppm): 163.58, 139.96, 137.53, 132.11, 130.46, 129.18, 129.00 128.20, 121.17, 105.91, 54.11. HR-ESI MS calcd for $C_{22}H_{18}N_6O$ 382.15 (**1**$^{+}$, 100%), found 383.1622 *m/z* ([**1**+ H^+]$^+$), 405.1445 *m/z* ([**1**+ Na^+]$^+$) and found 315.1283 *m/z* ([**1**- pyrazol]$^+$).

*2.3. Preparation of sensor **1** and metal ion solutions*

The stock solution of sensor **1** was prepared in acetonitrile with the concentration of 1×10^{-4} M and further diluted according to the actual requirements.

The solutions of metal ions with a concentration of 2×10^{-2} M in water were prepared using their inorganic salts, including nitrate salts (Fe^{3+}, Al^{3+}, Mg^{2+}, K^+, Cd^{2+}, Co^{2+}, Cr^{3+}, Zn^{2+} and Ag^+), chloride salts (Cu^{2+}, Cu^+, Hg^{2+}, Ni^{2+}, Pb^{2+}, Ca^{2+}, Mn^{2+}, Ba^{2+}, Na^+) and $FeSO_4\cdot7H_2O$.

*2.4. Detection of sensing properties of sensor **1** for copper ions*

2.4.1. Selective experiment

Both absorbance and fluorescence spectra were used to investigate the selective response of sensor **1** towards metal ions. The different metal ion in water solutions (20 equiv. of sensor **1)** were added with pipette into sensor **1** solution (1×10^{-5} M), respectively. After mixing them for 10 s, UV–vis absorbance and fluorescence spectra were taken at room temperature.

2.4.2. Fluorescence titration

For each titration solution with different molar ratio of Cu^{2+} to sensor **1** was prepared by adding different volumes [μL] of Cu^{2+} solution to sensor **1** solution (1×10^{-5} M), the maximum added volume of the metal ion solution did not exceed 2% volume of sensor **1** solution in order to avoid the effect of concentration on fluorescence spectra. The concentration of sensor **1** in every solution was kept at 1×10^{-5} M. The fluorescence spectra were taken at room temperature after finishing the solution preparation for 10 s.

2.4.3. Job's plot measurement

The stoichiometry of complexes can be obtained using Job's plot via the measurement of fluorescence spectra. Job's plot was drawn based on the measurement of a series of solutions in which the molar concentrations of ligand and metal ion vary but their sum remains constant. The fluorescence spectrum of each solution is measured and then the maximum value of emission was plotted against the mole

fraction of ligand or metal ion. The maximum on the Job's plot appear at the mole ratio corresponding to the combining ratio of the complex.

3. Results and discussion

3.1. Crystal growth and X-ray crystallography

The molecular structure of sensor **1** was also confirmed by the single crystal analysis. The colorless sensor **1** crystals with the size of 0.13 mm × 0.11 mm × 0.10 mm were obtained by slow evaporation method in DMSO after 6 days. Single-crystal X-ray diffraction data for sensor **1** were recorded using a Bruker Apex CCD diffractometer with graphite monochromated Mo Kα radiation (λ= 0.71073˚A) at 293 K. Absorption corrections were applied using a multi-scan technique. The structure was solved by direct method of SHELXS-97 and refined by full-matrix least-squares techniques using the SHELXL-97 program [26] within WINGX [27].

All non-hydrogen atoms were easily found from the Fourier difference maps and refined with anisotropic temperature parameters. The hydrogen atoms were generated geometrically. A summary of the crystal data, structure solution and refinement is provided in Table S1.

Single-crystal X-ray structural analysis reveals that sensor **1** crystallized in the orthorhombic space group *Pca2(1).* As shown in Fig. 1a, the crystal structure of sensor **1** consists of two parts, 2,5-Diphenyl-1,3,4-Oxadiazole and 1-methyl-1H-pyrazole. Adjacent molecules are packed together through π-π interactions (Fig. 1b) between the 1,3,4-oxadiazole groups and the phenyl groups [the distances of centroid-

to-centroid and centroid-to-plane (based on the phenyl groups) are 3.62 and 3.54 Å, respectively]. Then, the molecules are packed against each other through weak interactions to afford fascinating supramolecular layers (Fig. 1c).

Crystallographic data for the structure reported in this paper has been deposited with the Cambridge Crystallographic Data Centre, CCDC no. 1559079. Copies of this information are obtained free of charge from the Director, CCDC, 12 UNION Road, Cambridge 1EZ, UK (fax: 44 01223 336033, deposit@ccdc.cam.ac.uk or http://www.ccdc.cam.ac.uk).

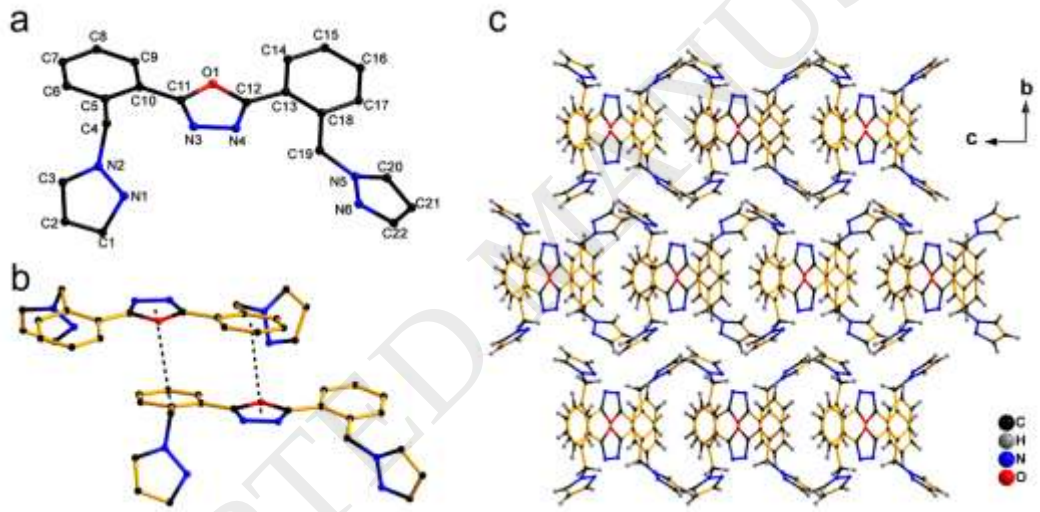

Fig.1. (a) View of the crystal structure of sensor **1** molecule. (b) View of the π-π interactions between two sensor **1** molecules. (c) View of the packing structure of sensor **1** along the *a* axis.

3.2. Photophysical properties (absorption and fluorescence spectra)

The absorbance and fluorescence spectra of sensor **1** in CH_3CN solution are shown in Fig. 2. The absorption band between 270~325 nm with the maximum absorption peak at 279 nm and emission band between 300～470 nm with maximum emission peak at 352 nm (λ_{ex} = 270 nm) of sensor **1** are at similar wavelength range with its

parent compound 3 in scheme 1. This result indicated that the absorbance and emission originated from oxadiazole group of sensor **1**. The quantum yield (Φ_F) of sensor **1** was 0.33, determined at room temperature using quinine sulfate (Φ_F=0.55 in 0.05 mol/L H_2SO_4) as standard [28]. The Φ_F showed that the sensor **1** is a candidate as fluorescence material.

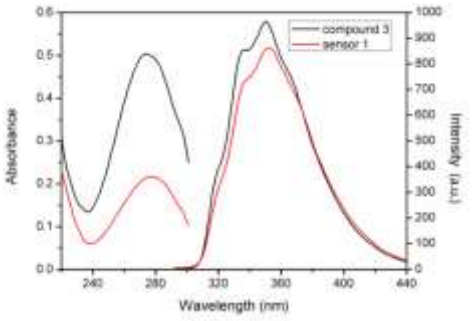

Fig.2. The comparison of fluorescence and absorbance spectra of sensor **1** and compound 3 in CH_3CN solutions.

*3.3. UV-vis absorbance spectra of sensor **1** with metal ions and colormetric sensing to Cu^{2+}*

There are two pyrazoles in sensor **1** molecule and the nitrogen atoms on pyrazole have the capability to coordinate with metal ions. According to our previous works [24-25], it is anticipated that sensor **1** could selectively coordinate with metal ions via the pyrazole units and further influence the absorbance and fluorescence spectra of oxadiazole unit.

First of all, the recognition properties of sensor **1** towards different metal ions including Fe^{3+}, Al^{3+}, Mg^{2+}, K^+, Cu^+, Cd^{2+}, Co^{2+}, Cr^{3+}, Zn^{2+}, Ag^+, Cu^{2+}, Hg^{2+}, Ni^{2+}, Pb^{2+}, Ca^{2+}, Mn^{2+}, Ba^{2+}, Na^+ and Fe^{2+} were investigated by visual detection

experiments. After addition of different metal ions (20 equiv. of sensor **1**) to the sensor **1** solution in CH_3CN (1×10^{-5} M), only the solution containing Cu^{2+} of sensor **1** turned from colorless to yellow straightway, shown in Fig. 3a. The result indicated that the sensor **1** can recognize Cu^{2+} selectively.

The color changes of sensor **1** solutions upon the addition of Cu^{2+} were further illustrated by the absorbance spectra, seen in Fig. 3b. The addition of Cu^{2+} enhanced the absorbance intensity of sensor **1** to 2-fold with a slightly red-shift to 285 nm. On the contrary, the other metal ions did not cause the obvious spectra changes, except that Fe^{3+} induced the increase of absorbance of sensor **1** to some content. This result was consistent with the color change of sensor **1** solution, upon the addition of Fe^{3+}, the color of sensor **1** solution displayed a slight yellow, shown in Fig. 3a. Another particular case is the addition of Hg^{2+}, a new absorbance peak at 240 nm appeared, but the absorption intensity at 279 nm did not change and the color of solution did not present obvious change. The blank experiment that the same amount of Hg^{2+} was added into acetonitrile without sensor **1** demonstrated that the absorbance peak at 240 nm come from the interaction of Hg^{2+} and acetonitrile (Fig. S4). So the addition of Hg^{2+} would not affect the detection of Cu^{2+}. Above consequence confirmed sensor **1** could be used as a colorimetric sensor of Cu^{2+} with high selectivity and sensitivity. The obvious change of the color and absorption intensity of sensor **1** upon the addition of Cu^{2+} was attributed to the complexation between the electron-donating pyrazoles and acceptor Cu^{2+}. On the contrary, other competitive metal ions did not form stable complexes and cause the negligible change of the absorption intensity, which may be due to the unsuitable coordination geometry conformation of the two pyrazoles in sensor **1** and the inappropriate ion radius and insufficient binding energy of these metal ions. The

colors change of the solutions from shallow to deep yellow was illustrated by the absorbance titration experiment of sensor 1 (1×10^{-5} M) with Cu^{2+} (0~40 equiv) in CH_3CN solution, as shown in Fig. S5. Upon gradual increasement of Cu^{2+}, the absorption intensity of the solution at 290 nm increased gradually.

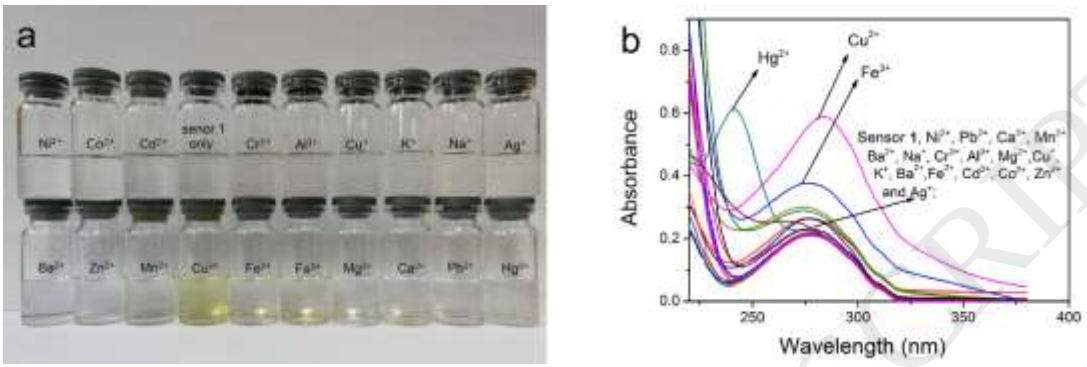

Fig.3. (a) The photographs of sensor **1** solutions containing different metal ions. (b) The absorbance spectra of sensor **1** in CH_3CN solution and different metal ions. In every sample, the concentration of sensor **1** is 1×10^{-5} M and the metal ion is 20 equiv. of sensor **1**. (For interpretation of the reference to color in this figure legend, the reader is referred to the web version of this article.)

The colorimetric sensing ability of sensor **1** to Cu^{2+} can be realized via the following manner. The series of standard solutions with constant concentration of sensor **1** (1×10^{-5} M) and different concentration of Cu^{2+} in CH_3CN were prepared, their yellow color gradually deepened with the concentration of Cu^{2+} (Fig. 4a). When the water sample was added into sensor **1** solution and the color would be compared with the above series of standard solutions, the concentration of Cu^{2+} in water sample could be evaluated roughly.

The competitive experiments could further confirmed the selectivity of sensor **1** to Cu^{2+}. Therefore, the competitive experiments were carried out by measurement of the absorbance spectra of the series of sensor **1** in CH_3CN solutions (1×10^{-5} M)

containing 20 equiv. of Cu^{2+} and 20 equiv. of the other metal ions. As shown in Fig. 4b, the ordinate values are the absorbance at 279 nm. This column diagram obviously showed that other coexistent competition cations had no influence on the colorimetric sensing of the sensor **1** to Cu^{2+}, which also confirmed the high colorimetric selectivity of sensor **1** to the Cu^{2+}.

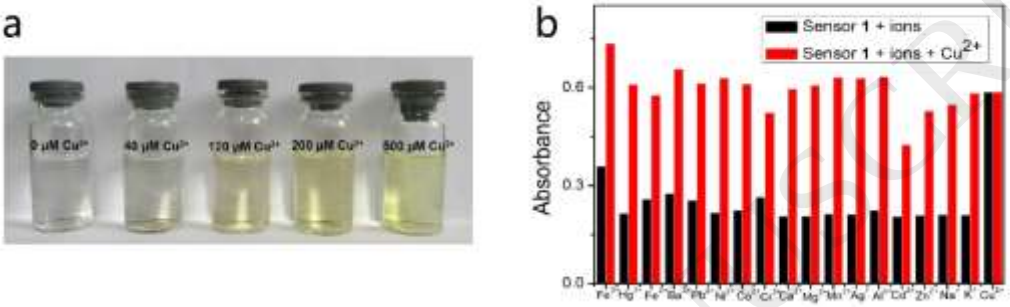

Fig.4. (a) Naked eye detection of sensor **1** to Cu^{2+} (concentration of sensor **1** is 1×10^{-5} M). (b) Selectivity of sensor **1** (1×10^{-5} M) in CH_3CN solution over other competitive metal ions (20 equiv. of sensor **1**). (For interpretation of the reference to color in this figure legend, the reader is referred to the web version of this article.)

*3.4. Fluorescence sensing of sensor **1** to Cu^{2+}*

Based on the absorbance properties of sensor **1** with metal ions, it is predicted that sensor **1** could selectively fluorescence sensing towards to Cu^{2+} over other competitive metal ions.

High selectivity toward target metal ion over the other potentially competitive ions is a very important parameter to evaluate the nature of a chemosensor. The selectivity of sensor **1** towards metal ions was investigated in different solvent systems including DMSO, CH_3CN, DMSO:H_2O (1:1, V:V), THF:H_2O (1:1, V:V) and CH_3CN:H_2O (1:1, V:V). Sensor **1** displayed satisfied result only in pure CH_3CN,

which may be ascribed to the weak solubility in aqueous solution. Although the metal ions detection was in CH_3CN solutions, the metal ions were in pure water solutions, so this method can be applied in the detection of metal ions in water. Therefore, the fluorescence response of sensor **1** towards various metal ions (20.0 equiv.) was tested in CH_3CN solution (1×10^{-5} M). Sensor **1** emitted blue fluorescence emission and presented strong fluorescence emission peak at 352 nm when it was excited at 270 nm. Most metal ions such as Fe^{3+}, Al^{3+}, Mg^{2+}, K^{+}, Cd^{2+}, Co^{2+}, Cr^{3+}, Zn^{2+}, Ag^{+}, Hg^{2+}, Ni^{2+}, Pb^{2+}, Ca^{2+}, Mn^{2+}, Ba^{2+}, Na^{+} and Fe^{2+} only induced negligible decrease in fluorescence spectra of sensor **1**. Only Cu^{2+} intensively impacted the fluorescence spectra of sensor **1** and quenched the fluorescence at a significant extent (Fig. 5a), the fluorescence intensity at 352 nm was quenched by 71% after addition of 20.0 equiv. Cu^{2+}, the fluorescence changed from “on” to “off”. The fluorescence images in Fig. 5b also proved the quenching phenomenon of Cu^{2+} on the fluorescence of sensor **1**, the fluorescence of sensor **1** was obviously quenched. These observations indicated that sensor **1** had excellent fluorescence selectivity to Cu^{2+} ion in CH_3CN solutions. The fluorescence of sensor **1** was quenched due to the forming of sensor **1**-Cu^{2+} complexes, the molecule of sensor **1** and Cu^{2+} ion was close-connected in complex structure and the paramagnetic properties of Cu^{2+} quenched the fluorescence of sensor **1**. This is ascribed to the unpaired d (9) electrons of Cu^{2+} ions, the electron transfer between the excited states of oxadiazole and the d-orbitals of copper ions took place. This process can effectively quench the excited states of the oxadiazole and further

quenched the fluorescence. This quenching mechanism is same as the many previous reports [29-33].

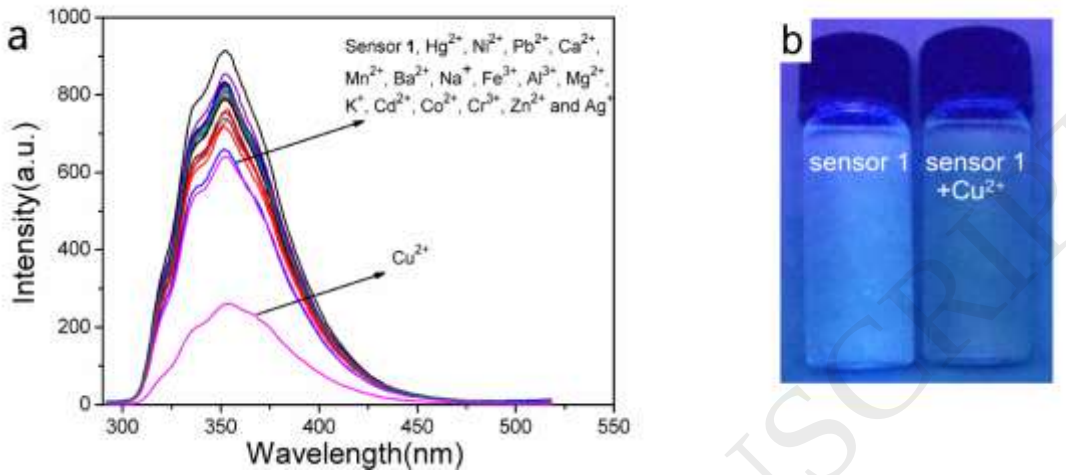

Fig.5. (a) Fluorescence response of sensor **1** (1×10^{-5} M) in CH_3CN towards to various metal ions (20.0 equiv.). (b) Fluorescence images of sensor **1** after addition of 20 equiv. Cu^{2+}. (For interpretation of the reference to color in this figure legend, the reader is referred to the web version of this article.)

Fast response of sensor **1** to Cu^{2+} is more suitable for real-time detection in practical samples. The experiment found that the fluorescence was instantly quenched to equilibrium point after addition of Cu^{2+} into sensor **1** solution within 10 seconds, so the synthesized sensor **1** could meet the requirement of real-time detection.

The reversibility of fluorescence response process of sensor **1** toward Cu^{2+} was also investigated with ethylenediaminetetraacetic acid disodium salt ($EDTANa_2$). After addition of excess EDTA (2 equiv. of Cu^{2+}) to sensor **1** (1×10^{-5} M) and Cu^{2+} (20 equiv. of sensor **1**) solution, the fluorescence spectrum of the resulted solution restored to the original spectrum of sensor **1** (Fig. S6), which indicates that the Cu^{2+} recognition is a complexing and reversible process.

The anti-jamming ability is also important for one fluorescence sensor to be used in practical applicability, the possible interference ions including Fe^{3+}, Al^{3+}, Mg^{2+}, K^{+}, Cd^{2+}, Co^{2+}, Cr^{3+}, Zn^{2+}, Ag^{+}, Hg^{2+}, Ni^{2+}, Pb^{2+}, Ca^{2+}, Mn^{2+}, Ba^{2+}, Na^{+} and Fe^{2+} were measured through competitive experiments. The competition experiment was carried out by monitoring the change of fluorescence intensity at 352 nm upon addition of 20 equiv. Cu^{2+} and 20 equiv. other metal ions to a solution of sensor **1**, the results are shown in Fig. 6a. The solutions of sensor **1** both containing addition of Cu^{2+} and different coexistent cations displayed significant fluorescence quenching and the quenching efficiencies (F_0-F/F_0) are the basically same as that caused by Cu^{2+} only. The fluorescence selectivity of sensor **1** was similar with the result of competitive experiment of UV-vis spectroscopy. These results indicated that sensor **1** had the capability of fluorescence recognition of Cu^{2+} ion with high selectivity and was not influenced by the coexisting metal ion.

The stoichiometry of sensor **1**-Cu^{2+} complex was determined by Job's plot method. As shown in Fig. 6b, the emission intensity at 352 nm was plotted against the fraction of Cu^{2+} under a constant total concentration (10 μM) of sensor **1** and Cu^{2+}. The Job's plot with a maximum at 0.5 molar fraction indicated 1:1 binding stoichiometry of sensor **1** and Cu^{2+} [34].

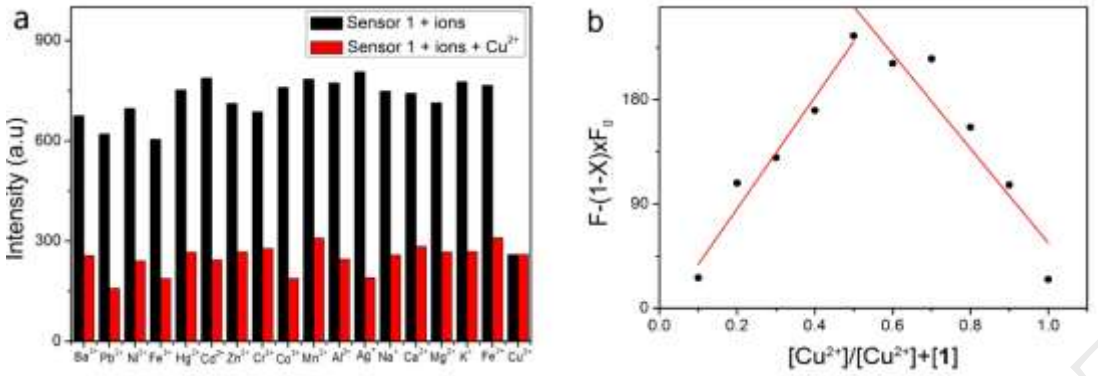

Fig.6. (a) The fluorescence intensity changes of sensor **1** (1×10^{-5} M) to various metal ions. The black bars represent the fluorescence intensity of sensor **1** in the presence of miscellaneous metal ions (20 equiv.), the red bars represent the fluorescence intensity of the above solution upon further addition of 20 equiv. of Cu^{2+} (λ_{em} = 352 nm). (b) Job's plot from the fluorescence emission spectra of sensor **1** and Cu^{2+} in CH_3CN solution with the total concentration of 10 μM. λ_{ex} = 270 nm, λ_{em} = 352 nm.

In order to evaluate the sensing properties of sensor **1** towards Cu^{2+}, fluorescence titration experiment of sensor **1** (1×10^{-5} M) with Cu^{2+} (0~50 equiv) in CH_3CN solution was carried out. The fluorescence intensity of sensor **1** at 352 nm was gradually quenched with the continuous growing concentration of Cu^{2+} from 0 to 0.5 mM (Fig. 7a). When the concentration of Cu^{2+} reached about 50.0 equiv of sensor **1**, the fluorescence intensity of sensor **1** decreased from 855 to 70 and the fluorescence was almost quenched.

The binding constant for the interaction of sensor **1** with Cu^{2+} ion was estimated using the data obtained in fluorescence titration studies. The association constant (K_a) for the sensor **1**-Cu^{2+} complex was evaluated using the Benesi-Hildebrand (B-H) plot according to the following equation [35].

$$1/(F_0\text{-}F) = 1/\{K_a(F_0 - F_{min})C\}+1/(F_0 - F_{min})$$

Where F_0 and F denoted the fluorescence intensities of sensor **1** only and in the presence of Cu^{2+}, C is the concentration of Cu^{2+} solution. F_{min} is the minimum fluorescent intensity at 352 nm in the presence of Cu^{2+}. Linear fitting of the experiment plot based on the 1:1 binding stoichiometry of sensor **1** and Cu^{2+} was examined and the fitted curve was almost superimposed over the experimental plot with a correlation coefficient over 0.98003 (Fig. 7b), which confirmed the 1:1 binding stoichiometry of sensor **1** and Cu^{2+}. K_a was obtained from the slope and intercept of the linear plot. In this way, the association constant was calculated to be K_a = 4.38×10^4 M^{-1}.

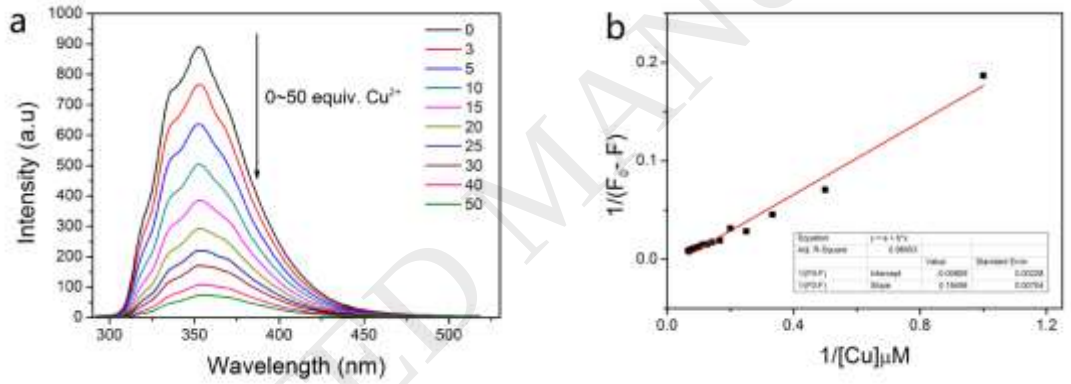

Fig. 7. (a) Fluorescence response of sensor **1** in CH_3CN solution (1×10^{-5} M) upon addition of Cu^{2+} (0~50 equiv.). λ_{ex} = 270 nm, λ_{em} = 352 nm. (b) Benesi-Hildebrand plot of sensor **1** (1×10^{-5}) in CH_3CN solution in the presence of Cu^{2+} (0~15 μM)) (R^2=0.98003).

Additionally, the fluorescent detection limit (LOD) of sensor **1** for Cu^{2+} was also obtained from the calibration curve of titration experiment (Fig. S7). The calibration curve of the fluorescence intensity at 352 nm versus [Cu^{2+}] displayed a linear graph and the regression coefficient was 0.99342. The detection limit was calculated to be 2.14 μM from the equation (3σ/K) [36], which is much lower than the limit of copper in drinking water (~20 μM) permitted by US Environment Agency (EPA) [37].

3.5. Stern-Volmer analysis

Stern-Volmer analysis was used to study the nature of the fluorescence quenching or enhancement process in the complexation of metal ions. The plots obtained emission intensities (F_0/F or lnF_0/F) against Cu^{2+} ion concentration and showed a linear graph [38].

$$\frac{F_0}{F} = 1 + K_{SV}[M] \quad \text{dynamic quenching}$$

$$\ln\frac{F_0}{F} = e^{K_{SV}[M]} \quad \text{static quenching}$$

F_0 and F are the fluorescence intensity of sensor **1** at 352 nm under the absence and presence of Cu^{2+}, respectively. K_{sv} is the Stern-Volmer quenching constant and [M] is the concentration of Cu^{2+}. As seen in Fig. 8, under the low concentration, F_0/F (black line) was not linear with quencher (Cu^{2+}) concentration, and thus failed to obey the Stern-Volmer model of dynamic quenching. However, the lnF_0/F values were linear with quencher concentration, the fitting linear relationship R^2 was 0.99699. This result was in agreement with the Perrin model of static quenching (blue line), suggesting that all the added quencher (Cu^{2+}) were bound to sensor **1**, and the quenched sensor **1** molecules lied within the quencher's active sphere. This result met the Perrin model which further supports that fluorescence quenching in this systems occurs intramolecularly.

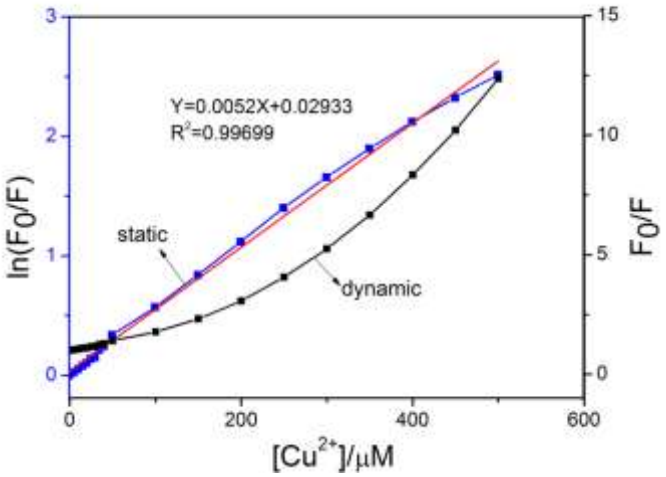

Fig.8. Stern-Volmer quenching constant analysis plots for dynamic quenching and static quenching of sensor **1** by Cu^{2+}.

3.6. Proposed mechanism

To further clarify the coordination behavior of sensor **1** with Cu^{2+}, density functional theory (DFT) calculations at the *B3LYP/6-31G(d)* level of Gaussian 09 package [39] were carried out to provide a theoretical basis on the mechanism of interaction between sensor **1** and Cu^{2+}. The optimized ground-state geometries in Fig. 9a revealed a 1:1 binding stoichiometry of sensor **1** and Cu^{2+} ion. There were two coordination bonds between Cu^{2+} and nitrogen atoms in pyrazoles via the lone pairs of nitrogen atoms.

The frontier orbital energies and shapes can help us to get more insight into the interaction of sensor **1** with Cu^{2+}. As can be seen from Fig. 9b, both HOMO and LUMO of sensor **1** were mainly centered on the oxadiazole moiety and benzene ring, while the HOMO of sensor **1**-Cu^{2+} complex was localized in whole molecular backbone. On the other hand, the energy gap between the HOMO and LUMO of

sensor **1**-Cu^{2+} was calculated to be 1.40 eV, which was much smaller than that of sensor **1** (4.83 eV). A molecule with high HOMO energy will be more unstable and is easy to react. These results suggested the frontier molecular orbitals of sensor **1**-Cu^{2+} complex were better stabilized than those of sensor **1**. The above explanation based on DFT had also confirmed 1:1 binding mode of sensor **1**-Cu^{2+} complex.

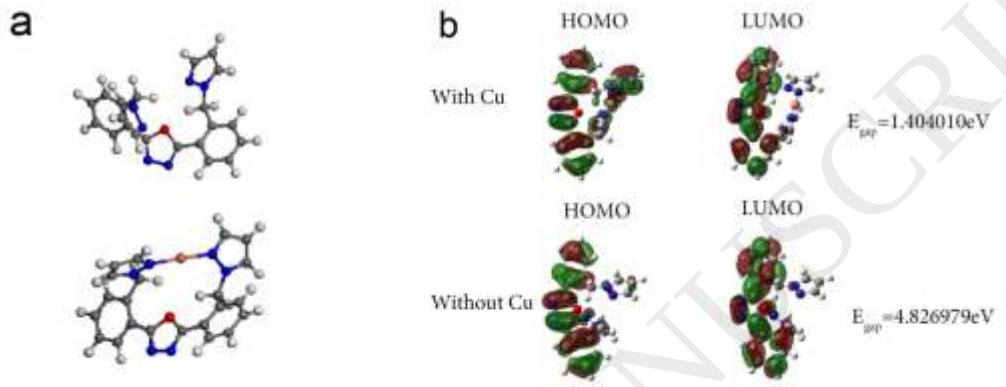

Fig.9. (a) Optimized ground-state geometries of sensor **1** and senor 1- Cu^{2+}. Color code: C (black), N (blue), H (white), O (red), Cu^{2+} (orange). (b) Frontier orbital shapes of sensor **1** and sensor **1**-Cu^{2+} complex.(For interpretation of the reference to color in this figure legend, the reader is referred to the web version of this article.)

Above results of spectral studies suggested that the sensing behavior of sensor **1** towards Cu^{2+} ion involves the formation of a 1:1 complex. The fluorescence of sensor **1** was quenched because of the paramagnetic properties of Cu^{2+} via the forming of sensor **1**-Cu^{2+} complexes. The excess solid Cu^{2+} salt was added into sensor **1** solution in DMSO-d_6, after enough mixing and complexes formation, the upper clear solution was used in ESI-mass spectrometry analysis. As shown in Fig. S8, ESI-mass spectra gave a molecular-ion peak at *m/z* = 445.1486 belonged to [**1**+Cu^{2+}-H^+]$^+$ species. Additionally, the other molecular-ion peak at *m/z* 479.1141 appeared in mass spectra, which matched with the complex corresponded to [**1**+Cu^{2+}+Cl^--2H^+] and indicated Cl^-

ion participated in the coordination reaction with Cu^{2+}. These results demonstrated the formation of complexes between sensor **1** and Cu^{2+} with 1:1 stoichiometry.

To further demonstrate the complex effect of sensor **1** and Cu^{2+}, ^1H NMR titration of sensor **1** and Cu^{2+} in DMSO-d_6 were conducted. As shown in Fig. 10, the integration and peak shifts of spectra afforded the obvious evidence of the proposed binding mode. The peaks at 6.34, 7.54 and 7.88 ppm were corresponded to the proton H_a and H_b of pyrazole rings and H_c of benzene ring separately. With the addition of Cu^{2+} to the solution of sensor **1**, sensor **1**-Cu^{2+} complex was gradually formed. Consequently, the proton signal of H_a, H_b and H_c displayed significant downfield shift with a gradual broadening. At the existence of 2.0 equiv. Cu^{2+} ion, these proton signals almost merged with the base line and disappeared. These observations clearly indicated that the nitrogen atoms on pyrazole were the binding sites for Cu^{2+}.

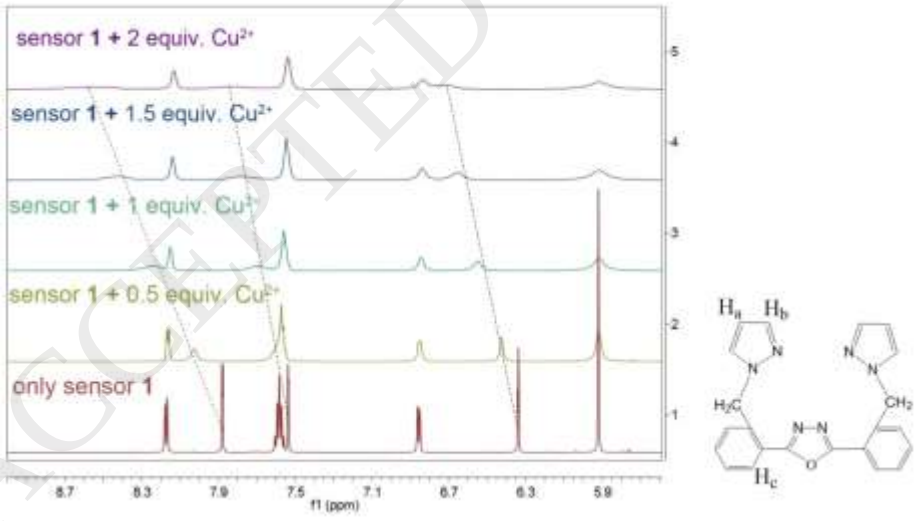

Fig.10. ^1H NMR titration experiment of sensor **1** in the presence of different amounts of Cu^{2+} in DMSO-d_6.

Based on the above results, the binding mode of sensor **1** with Cu^{2+} and fluorescence quenching mechanism were proposed in Scheme 2.

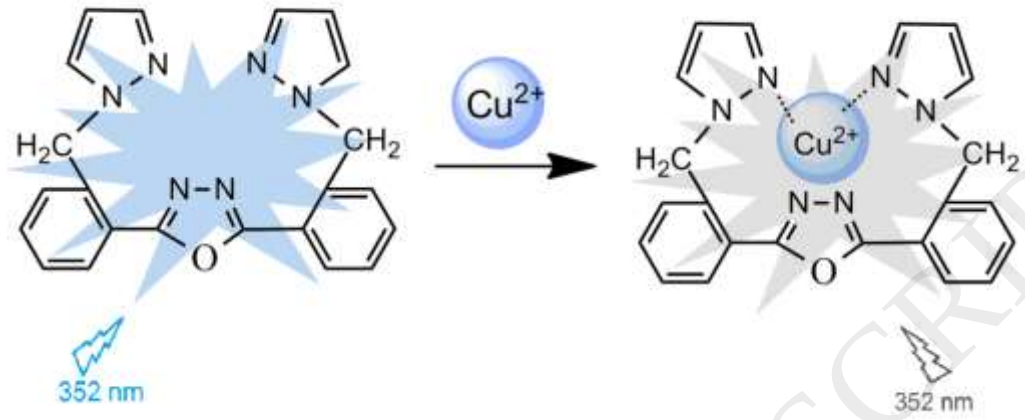

Scheme 2. The proposed mechanism for Cu^{2+} detection by sensor **1**.

4. Conclusions

Herein we report a highly selective and sensitive "on-off" fluorescent chemosensor based on oxadiazole and pyrazole for Cu^{2+} in presence of coexisting metal ions. The fluorescence quenching was caused by the complex formation between sensor **1** and Cu^{2+}, the fluorescence and ^1H NMR titrations, ESI-mass and DFT calculation evidenced the sensor **1**-Cu^{2+} complex with 1:1 stoichiometry. Sensor **1** also displayed the naked-eye detection capability for Cu^{2+} via the color change from colorless to yellow. Both fluorescent and colorimetric sensing of sensor **1** towards Cu^{2+} displayed high sensitivity and selectivity, and also was not interfered by the co-existence of other metal ions. Sensor **1** displayed great potential for detection for Cu^{2+}, so we hope these results will promote the rational design for a more excellent chemosensor for Cu^{2+} in the future.

Acknowledgement

This work was supported by the National Natural Science Foundation of China (no. 50873019) and Research Fund for the Doctoral Program of Higher Education of China (20120043110007).

References

[1] Linder M-C; Hazegh-Azam M; *Am. J. Clin. Nutr.* **1996**, 63, 797.

[2] Uauy R; Olivares M; Gonzalez M; *Am. J. Clin. Nutr.* **1998**, 67, 952.

[3] Puig S; Thiele D-J; C*urr Opin Chem Biol.* **2002**, 6, 171.

[4] Tan Y. F; O'Toole N; Taylor N. L; Millar A. H; *Plant physiology* **2010**, 152(2), 747.

[5] Desai V; Kaler S-G; *Am. J. Clin. Nutr.* **2008**, 88, 855.

[6] Shoaee H; Roshdi M; Khanlarzadeh N; Beiraghi A; *Spectrochim. Acta, Part A* **2012**, 98, 70.

[7] Gaubeur I; Aguirre MA; Kovachev N; Hidalgo M; Canals A; *Microchem. J.* **2015**, 121, 219.

[8] Giersz J; Bartosiak M; Jankowski K; *Talanta* **2017**, 167, 279.

[9] Özzeybek G; Erarpat S; Chormey DS; Fırat M; Büyükpınar Ç; Turak F, et al; *Microchem. J.* **2017**, 132, 406.

[10] Li Y; Zhang X; Zhu B; Xue J; Zhu Z; Tan W; *The Analyst*. **2011**, 136(6), 1124.

[11] Grujicic D; Pesic B; *Electrochim. Acta* **2002**, 47, 2901.

[12] Li W; Zhu G; Li J; Wang Z Jin Y; *Molecules* **2016**, 21(1), E107.

[13] Li L.L; Li H; Liu G; Pu S.Z; *J Photoch Photobio A* **2017**,338(1), 192.

[14] Tomoya H; Yuki N; Takuya S; Mari I.Y; Hiroyuki K; *Tetrahedron* **2016**,72,4925.

[15] Yin J; Bing Q.J; Wang L; Wang G; *Spectrochim. Acta, Part A* **2018** 189, 495.

[16] Wang Y; Chang H.Q; Wu W.N et al.; *J Photoch Photobio A* **2017**,335, 10.

[17] Hidetomo Y; Ayumi O; Hiroyuki K; Tomoya H; *Tetrahedron* **2016**,72,5872.

[18] Liu Q; Huo R; Wei D; Zhao X; Zhao Z; Cai K; *Dyes Pigm* **2017**, 139, 1.

[19] Fabiane S.C; Marcelo C.N; Leonardo B; Guilherme S.M; Fábio S.N; *J Photoch Photobio A* **2017**,348(1), 41.

[20] Kaur M; Cho MJ; Choi DH; *Dyes Pigm* **2016**, 125, 1.

[21] Zeng J.R; Cheng C.C; Chang C.J; Huang C.H; Chen J.K; *Dyes Pigm* **2017**, 139, 300.

[22] Jing YM; Zhao Y; Zheng YX; *Dalton T* **2017**, 46(3), 845.

[23] Paun A; Hadade N.D; Paraschivescu C.C; Matache M; *J. Mater. Chem. C* **2016**, 4(37), 8596.

[24] Zhu L; Gu C; He Y; Wang G; *J. Lumin.* **2014**, 153, 439.

[25] Zhang Y; Wang G; Zhang J; *Sens. Actuators, B* **2014**, 200, 259.

[26] Sheldrick G; *Acta Crystallogr Sect* A **2008**;64:112.

[27] Farrugia L.J; WINGX. A Windows Program For Crystal Structure Analysis, University of Glasgow, Glasgow, UK, **1988**.

[28] Venegas F; Pizarro N; Vega A; *J. Chil. Chem. Soc.* **2011**, 56, 823.

[29] Maria S; Claudio P; *Coord. Chem. Rev.* 2016, **318**, 16.

[30] Chang J.H; Choi Y.M; ShinY.K; *Bull. Korean Chem. Soc.* 2001, **22**, 527.

[31] Choi M.G; Cha S.Y; Lee H.K; Jeon H. L; *Chang S. K; Chem. Commun.* 2009, **47**, 7390.

[32] Zhang L; Lou X.D; Yu Y, Qin J.G; Li Z; *Macromolecules* 2011, **44**, 5186.

[33] Silvia M; Stefano M; Maria S; Claudio P; *Eur. J. Inorg. Chem.* 2015, **13**, 2272.

[34] Satheshkumar A; El-Mossalamy EH; Manivannan R; Parthiban C; Al-Harbi LM; Kosa S, et al; *Spectrochim. Acta, Part A* **2014**, 128, 798.

[35] Benesi HA; Hildebrand JH; *J. Am. Chem. Soc.* **1949**, 71, 2703.

[36] Tsui Y-K; Devaraj S; Yen Y.P; *Sens. Actuators, B* **2012**, 161(1), 510.

[37] Liu JW; Lu Y; *J. Am. Chem. Soc*. **2007**, 129, 9838.

[38] Nudelman R; Ardon O; Hadar Y; Chen YN; Libman J; Shanzer A; *J. Med. Chem.* **1998**, 41, 1671.

[39] Zhao B; Liu T; Fang Y; Wang L; Kan W; Deng Q, et al; *Sens. Actuators, B* **2017**, 246, 370.

Figure Caption:

Scheme 1. The synthetic route of sensor **1**

Scheme 2. The proposed mechanism for Cu^{2+} detection by sensor **1**.

Fig.1. (a) View of the crystal structure of sensor **1** molecule. (b) View of the π-π interactions between two sensor **1** molecules. (c) View of the packing structure of sensor **1** along the *a* axis.

Fig.2. The comparison of fluorescence and absorbance spectra of sensor **1** and compound 3 in CH_3CN solutions.

Fig.3. (a) The photographs of sensor **1** solutions containing different metal ions. (b) The absorbance spectra of sensor **1** in CH_3CN solution and different metal ions. In every sample, the concentration of sensor **1** is 1×10^{-5} M and the metal ion is 20 equiv. of sensor **1**. (For interpretation of the reference to color in this figure legend, the reader is referred to the web version of this article.)

Fig.4. (a) Naked eye detection of sensor **1** to Cu^{2+} (concentration of sensor **1** is 1×10^{-5} M). (b) Selectivity of sensor **1** (1×10^{-5} M) in CH_3CN solution over other competitive metal ions (20 equiv. of sensor **1**). (For interpretation of the reference to color in this figure legend, the reader is referred to the web version of this article.)

Fig.5. (a) Fluorescence response of sensor **1** (1×10^{-5} M) in CH_3CN towards to various metal ions (20.0 equiv.). (b) Fluorescence images of sensor **1** after addition of 20 equiv. Cu^{2+}. (For interpretation of the reference to color in this figure legend, the reader is referred to the web version of this article.)

Fig.6. (a) The fluorescence intensity changes of sensor **1** (1×10^{-5} M) to various metal ions. The black bars represent the fluorescence intensity of sensor **1** in the presence of miscellaneous metal ions (20 equiv.), the red bars represent the fluorescence intensity of the above solution upon further addition of 20 equiv. of Cu^{2+} (λ_{em} = 352 nm). (b) Job's plot from the fluorescence emission spectra of sensor **1** and Cu^{2+} in CH_3CN solution with the total concentration of 10 μM. λ_{ex} = 270 nm, λ_{em} = 352 nm.

Fig. 7. (a) Fluorescence response of sensor **1** in CH_3CN solution (1×10^{-5} M) upon addition of Cu^{2+} (0~50 equiv.). λ_{ex} = 270 nm, λ_{em} = 352 nm. (b) Benesi-Hildebrand plot of sensor **1** (1×10^{-5}) in CH_3CN solution in the presence of Cu^{2+} (0~15 μM)) (R^2=0.98003).

Fig.8. Stern-Volmer quenching constant analysis plots for dynamic quenching and static quenching of sensor **1** by Cu^{2+}.

Fig.9. (a) Optimized ground-state geometries of sensor **1** and senor 1- Cu^{2+}. Color code: C (black), N (blue), H (white), O (red), Cu^{2+} (orange). (b) Frontier orbital shapes of sensor **1** and sensor **1**-Cu^{2+} complex.(For interpretation of the reference to color in this figure legend, the reader is referred to the web version of this article.)

Fig.10. ^{1}H NMR titration experiment of sensor **1** in the presence of different amounts of Cu^{2+} in DMSO-d_6.